

Modulation of western North Pacific tropical cyclone activity by the Atlantic Meridional Mode

Wei Zhang^{1,2,5} · Gabriel A. Vecchi^{1,2} · Gabriele Villarini³ · Hiroyuki Murakami^{1,2} · Anthony Rosati¹ · Xiaosong Yang^{1,4} · Liwei Jia^{1,2} · Fanrong Zeng¹

Received: 22 November 2015 / Accepted: 19 March 2016 / Published online: 11 May 2016
© Springer-Verlag Berlin Heidelberg 2016

Abstract This study examines the year-to-year modulation of the western North Pacific (WNP) tropical cyclones (TC) activity by the Atlantic Meridional Mode (AMM) using both observations and the Geophysical Fluid Dynamics Laboratory Forecast-oriented Low Ocean Resolution Version of CM2.5 (FLOR) global coupled model. 1. The positive (negative) AMM phase suppresses (enhances) WNP TC activity in observations. The anomalous occurrence of WNP TCs results mainly from changes in TC genesis in the southeastern part of the WNP. 2. The observed responses of WNP TC activity to the AMM are connected to the anomalous zonal vertical wind shear (ZVWS) caused by AMM-induced changes to the Walker circulation. During the positive AMM phase, the warming in the North Atlantic induces strong descending flow in the tropical eastern and central Pacific, which intensifies the Walker cell in the WNP. The intensified Walker cell is responsible for the suppressed (enhanced) TC genesis in the eastern

(western) part of the WNP by strengthening (weakening) ZVWS. 3. The observed WNPTC–AMM linkage is examined by the long-term control and idealized perturbations experiment with FLOR-FA. A suite of sensitivity experiments strongly corroborate the observed WNPTC–AMM linkage and underlying physical mechanisms.

Keywords Tropical cyclone · Western North Pacific · Atlantic Meridional Mode

1 Introduction

Tropical cyclones (TCs) are among the most destructive and costly natural disasters (e.g., Rappaport 2000; Pielke et al. 2008; Zhang et al. 2009). Understanding and predicting the status of TC occurrence is a topic of intense scientific interest (e.g., Mitchell 1932; Gray 1979; Vitart and Stockdale 2001; Klotzback 2007; Vecchi et al. 2014).

Environmental factors affecting the status of TC genesis in the western North Pacific (WNP) are strongly modulated by the sea surface temperature (SST) modes such as the El Niño Southern Oscillation (ENSO) (e.g., Chan 1985; Wu and Lau 1992; Chan 2000; Wang and Chan 2002; Camargo and Sobel 2005; Zhang et al. 2012, 2015, 2016b), the North Pacific Gyre Oscillation (Zhang et al. 2013), the Pacific Meridional Mode (PMM) (Zhang et al. 2016a), the Pacific Decadal Oscillation (PDO; Lee et al. 2012; Liu and Chan 2012; Girishkumar et al. 2014) and basin-wide Indian ocean SST changes (Du et al. 2010; Zhan et al. 2010; 2014). Therefore, the SST patterns in both Pacific and other ocean basins can alter the occurrence of WNP TCs through both local forcing and remote teleconnections. A number of studies have documented the importance of the North Atlantic SST in mediating Pacific climate including

✉ Wei Zhang
wei.zhang@noaa.gov

¹ National Oceanic and Atmospheric Administration/ Geophysical Fluid Dynamics Laboratory, Princeton, NJ 08540, USA

² Atmospheric and Oceanic Sciences Program, Princeton University, Princeton, NJ 08540, USA

³ IIHR-Hydroscience and Engineering, The University of Iowa, Iowa City, IA, USA

⁴ University Corporation for Atmospheric Research, Boulder, CO, USA

⁵ Key Laboratory of Meteorological Disaster, Ministry of Education, and Collaborative Innovation Center on Forecast and Evaluation of Meteorological Disasters, Nanjing University of Information Science and Technology, Nanjing, China

the Walker circulation (England et al. 2014; McGregor et al. 2014), ENSO (Ham et al. 2013; Yu et al. 2014), and the PDO (Zhang and Delworth 2007; Zhang and Zhao 2015). The SST anomalies in the North Atlantic have been recently found to exhibit substantial statistical connection with WNP TC activity (Li et al. 2013; Huo et al. 2015; Yu et al. 2015). More specifically, positive SST anomalies in the North Atlantic tend to suppress TC activity in the WNP (Li et al. 2013; Huo et al. 2015; Yu et al. 2015). Yu et al. (2015) proposed the Indian Ocean relay effect for interpreting the link between North Atlantic SST anomalies and WNP TCs. Huo et al. (2015) analyzed observed statistical relationships between Atlantic SST and the key dynamic and thermodynamic conditions in the WNP to interpret the impacts of North Atlantic SST on WNP TCs; yet the underlying physical mechanisms connecting the Atlantic to these large-scale WNP changes were not provided in their study. Therefore, while there is mounting evidence supporting the idea that North Atlantic SST influences the occurrence of WNP TCs, the field is still attempting to disentangle the underlying physical mechanisms.

The Atlantic Meridional Mode (AMM) is a leading mode of the coupled ocean/atmosphere system in the tropical & subtropical Atlantic (Nobre and Shukla 1996; Chang et al. 1997; Chiang and Vimont 2004; Vimont and Kossin 2007; Smirnov and Vimont 2011). The AMM has also been referred to historically as the Atlantic Dipole or Inter-hemispheric Mode (Servain 1991; Xie and Philander 1994; Carton et al. 1996) or the tropical Atlantic gradient mode (Chiang et al. 2002). The AMM exhibits variability on a variety of time scales from inter-annual to decadal. On decadal scales, the AMM is closely linked to the Atlantic Multidecadal Oscillation (AMO) (Kossin and Vimont 2007; Vimont and Kossin 2007; Grossmann and Klotzbach 2009). While it has been shown that the AMM modulates hurricane activity in the North Atlantic (Vimont and Kossin 2007), here we examine whether, the extent to which and by what mechanisms changes in the phase and magnitude of AMM can modulate WNP TC activity. By using the long-term control experiments of the Geophysical Fluid Dynamics Laboratory (GFDL) Forecast-oriented Low Ocean Resolution Version of CM2.5 (FLOR), we can test the robustness of the observed linkage between WNP TC activity and AMM and explore the mechanisms behind the connection. This study will advance our understanding of TC activity in the WNP, and provide references for the prediction and projection of WNP TC activity.

The remainder of this paper is organized as follows. Section 2 presents methodology and Sect. 3 discusses the analysis results based on observation and simulation results. Section 4 includes the discussion and conclusion.

2 Data and methodology

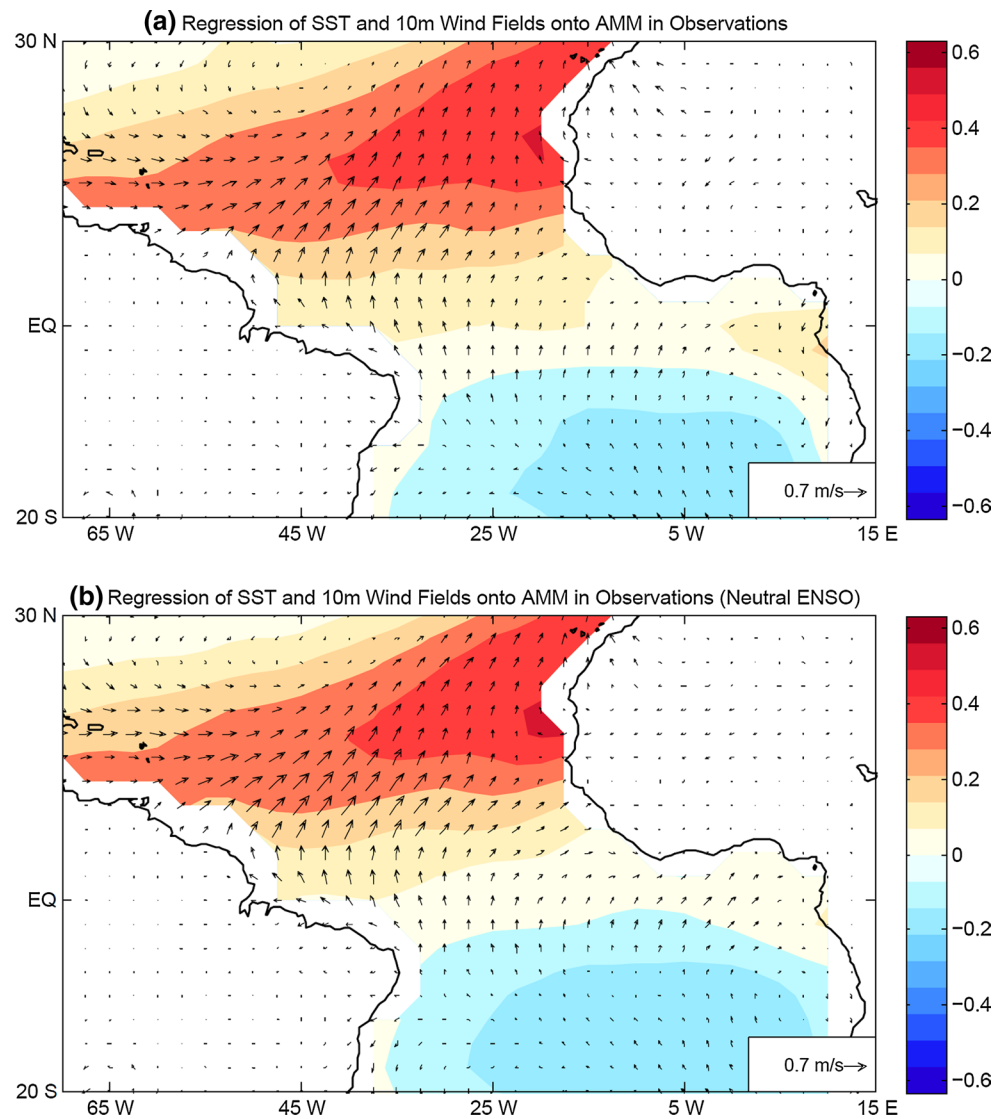
2.1 Data

The TC data are obtained from International Best Track Archive for Climate Stewardship (IBTrACS; Knapp et al. 2010) and the source of TC data for this study is from the Japan Meteorology Agency (JMA). The analysis results are consistent using four TC best track data [i.e., JMA, the Joint Typhoon Warning Center (JTWC), the Chinese Meteorology Administration (CMA) and the Hong Kong Observatory (HKO)]. We focus on WNP TCs that occur in the peak season (June to November: JJASON). The key meteorological variables such as zonal and meridional wind fields, geopotential height, vorticity and relative humidity are from the JMA 55 reanalysis data (JRA-55, Kobayashi et al. 2015). To substantiate the results, the National Centers for Environmental Prediction and the National Center for Atmospheric Research (NCEP/NCAR; Kalnay et al. 1996) reanalysis data are also used. The JRA-55 is available since 1958 on a global basis with a spatial resolution of $1.25^\circ \times 1.25^\circ$. It is based on a new data assimilation system that reduces many of the problems reported in the first JMA reanalysis (Kobayashi et al. 2015). The zonal vertical wind shear ($|\text{d}u/\text{d}z|$ or $|\text{d}u_z|$) is defined as the magnitude of the differences in zonal wind between 200 and 850 hPa level. Monthly estimates of SST are taken from the Met Office Hadley Centre HadSST3.1.1.0 (Kennedy et al. 2011).

2.2 AMM index

The AMM index is calculated following Chiang and Vimont (2004) by the singular value decomposition (SVD) of 10 m surface wind fields (zonal and meridional components) and SST. In its calculation, the seasonal cycle and the linear trend are first removed by applying a three-month running mean to the data, and then subtracting the linear fit to the cold tongue index (CTI, Deser and Wallace 1987) from every single spatial point to remove correlations with El Niño (Chiang and Vimont 2004). The CTI is defined as the average SST anomaly over 6°N – 6°S , 180 – 90°W (Deser and Wallace 1987). The regression of SST and 10 m surface wind fields onto the AMM index (i.e., the PC time series) represents the spatial patterns during the positive AMM phase (Fig. 1). The warming and cooling patterns of SST stride the equator and are coupled with surface winds (Fig. 1). To further validate the independence of AMM on ENSO, we also show the AMM pattern during neutral ENSO years (Fig. 1b). The El Niño (La Niña) years are defined as those with the Niño 3 values during June–November larger (smaller) than 1 (–1) standard deviation.

Fig. 1 The regression of SST (unit: °C) and 10 m wind fields (ms^{-1}) onto the AMM index in observations during **a** 1970–2013 and **b** neutral ENSO years in this period. The *blue* (*red*) shading represents negative (positive) SST anomalies



2.3 Global coupled model

This study employs a newly-developed high-resolution coupled climate model for experiments, the Geophysical Fluid Dynamics Laboratory (GFDL) Forecast-oriented Low Ocean Resolution Version of CM2.5 (FLOR) (e.g., Vecchi et al. 2014; Jia et al. 2015; Yang et al. 2015). This model is characterized by high-resolution land and atmosphere components but relatively low-resolution ocean component (Vecchi et al. 2014). The atmosphere and land are the same as those of the GFDL Climate Model version (CM) 2.5 (CM2.5; Delworth et al. 2012) with a spatial resolution of $50 \text{ km} \times 50 \text{ km}$. The ocean and sea ice components of FLOR are similar to those in the CM2.1 (Delworth et al. 2006) with a spatial resolution of $1^\circ \times 1^\circ$. The relatively low spatial resolution of the ocean and sea ice components in FLOR enables large ensembles and better efficiency for seasonal forecasting. This study utilizes the flux-adjusted

version of FLOR (FLOR-FA) for sensitivity experiments in which climatological adjustments are applied to the model's momentum, enthalpy and freshwater flux from the atmosphere to the ocean to give the model's SST and surface wind stress a closer climatology to the observations over 1979–2012 (Vecchi et al. 2014). For more details about the FLOR model, please refer to Vecchi et al. (2014), Jia et al. (2015), Yang et al. (2015) and references therein.

2.4 Control simulation

A 3500-year long control simulation was performed with the FLOR-FA by prescribing radiative forcing representative of 1860. These experiments are referred to as “Pre-industrial” experiments with FLOR-FA. Here we focus on the first 1000 years for the analysis of AMM and TCs for the sake of computing efficiency. We compared the results based on the first 1000 years from those derived from the

other 2500 years and the results are consistent. The 500-year control simulation by prescribing radiative forcing and land use representative of 1990 with FLOR-FA is also analyzed to characterize the AMM-TC association. Because the AMM-TC association based on FLOR-FA 1990 is consistent with that on FLOR-FA 1860, this study only shows results based on FLOR-FA 1860. TCs are tracked from the simulations of FLOR by a tracker described in the “Appendix”.

2.5 Perturbation experiments

A reference climatological experiment (CLIMO) is prepared by nudging the SSTs in FLOR to the repeating annual cycle of global climatological SST from the long-term control experiment of FLOR-FA; the perturbation experiment (PAMM) is designed by prescribing the annual cycle of climatological SST outside the AMM region and the overlapping of the annual cycle of climatological SST and SST anomalies associated with the positive AMM mode inside the AMM region. SST in both experiments is restored to each target with 5-day time scale. The subtraction of the control experiment from the perturbation experiment (PAMM minus CLIMO) produces the net influence of the positive AMM mode. Because GFDL FLOR is a TC-resolving model, we use a tracker to extract TCs from the simulated output. Both CLIMO and PAMM experiments spin up for 100 years and further integrated for 60 years.

3 Analysis results

3.1 Results from observations

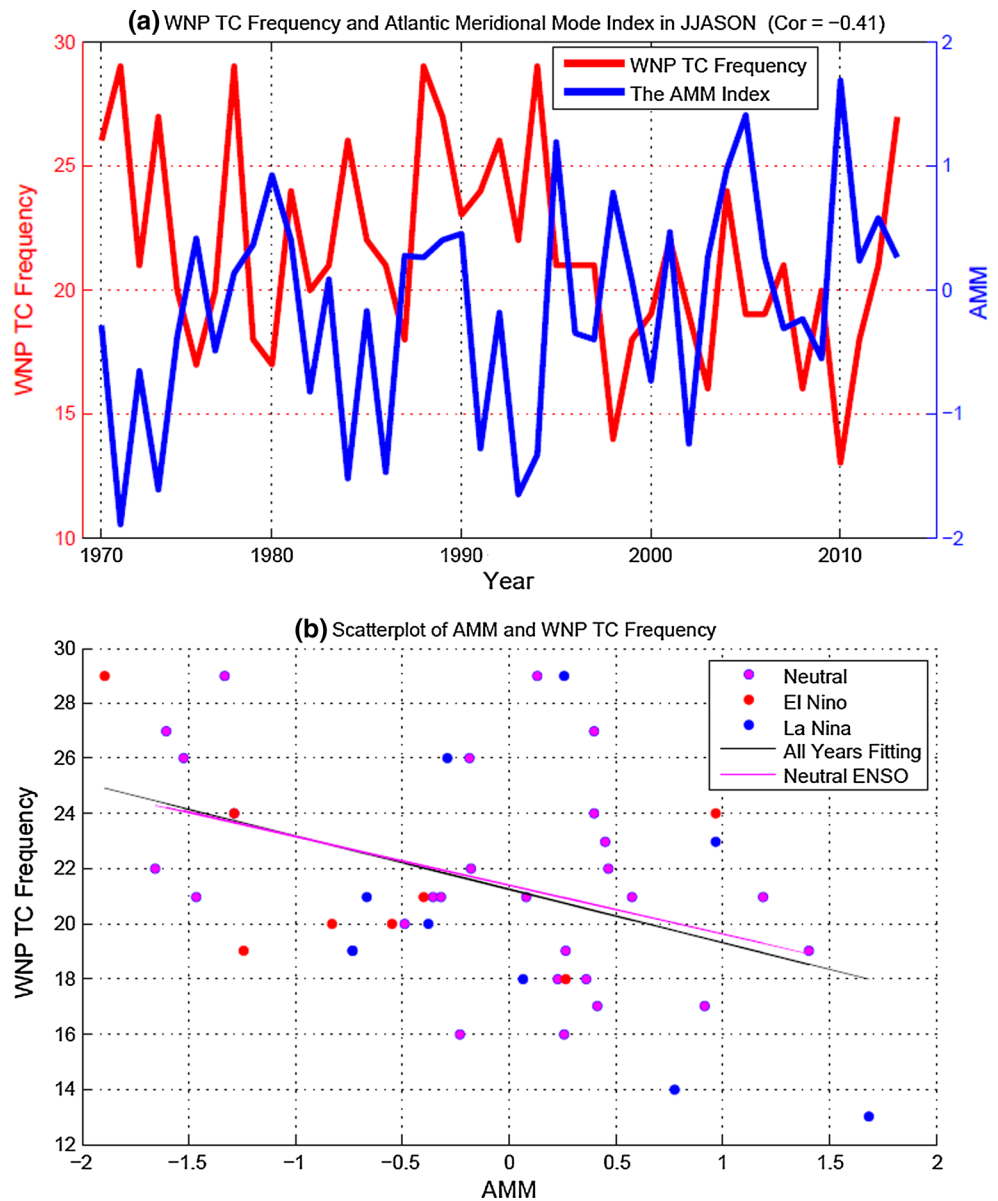
We start with the analysis of AMM which is derived from observed SST data. The full AMM index exhibits an increasing trend over 1970–2013, but we explore the detrended time series to focus on the year-to-year variations (Fig. 2a). The detrended AMM index has a significant correlation (-0.41) with WNP TC frequency for 1970–2013 at 0.01 level of significance, reflecting a tendency for WNP TC frequency to be suppressed (enhanced) in the positive (negative) AMM phase (Fig. 2a). We do not consider autocorrelation in the calculation of the correlation between the WNP TC frequency and the AMM index because the autocorrelations for WNP TC frequency and the AMM index are statistically insignificant. The slope of the linear least square fit line for all years (1970–2013) is almost the same as the one for only the neutral ENSO years during this period, indicating that the strong WNPTC-AMM association may not be directly caused by El Niño/La Niña events (Fig. 2b). However, the WNPTC-AMM association is to some degree affected by the warm/cold phase of ENSO (Fig. 2b).

More details of the relationship of the AMM with WNP TC can be seen in the regression of TC track density onto the detrended AMM index for the period 1970–2013, which shows negative loading in almost the entire WNP (Fig. 3a). In addition, the regression of TC genesis density onto AMM features negative anomalies in the WNP except the regions from 130°E to 145°E in the southwestern WNP (Fig. 3b). Moreover, the regression of basinwide TC genesis anomalies onto AMM is negative. The spatial regression of both WNP TC density and genesis onto the AMM index, along with the correlation of basinwide frequency with AMM, indicates a significant link between AMM and WNP TC activity. The southeastern part of the WNP has long been considered a key region for WNP TC genesis (Chan 2000; Wang and Chan 2002; Camargo et al. 2007a, b).

Previous studies have highlighted the dominant role of zonal vertical wind shear (ZVWS) induced by remote SST, instead of local SST, in modulating WNP TC genesis (Wang and Chan 2002; Chan and Liu 2004). The regression of TC genesis density onto AMM shows similarities with that of the genesis potential index (GPI) (Emanuel and Nolan 2004; Camargo et al. 2007a, b) (Figs. 3b, 4a). Specifically, the regression of GPI onto the AMM index is characterized by negative anomalies in the eastern WNP and positive anomalies in the western WNP (Fig. 4a). Among the factors associated with GPI, ZVWS stands out to agree with the spatial patterns of GPI while 600-hPa relative humidity and 850-hPa relative vorticity are not consistent with the spatial patterns of GPI (Fig. 4b, d). To further assess the underlying mechanisms, we analyze the Walker circulation, represented by the vertical profile of vertical pressure velocity and zonal wind averaged over 0–20°N where most of WNP TCs are formed. The anomalous ZVWS is associated with an anomalous regional Walker cell in the WNP (120°E–180°E) (Fig. 4e). An anomalously ascending (reduced subsidence) branch in the western WNP (120°E–150°E) is accompanied with an anomalously descending (reduced ascent) branch in the eastern WNP (150°E–180°E) (Fig. 4e). This anomalous zonal circulation would intensify ZVWS, and act to suppress TC activity in the eastern WNP during the positive AMM phase because the climatology of lower level and upper level winds are largely easterly and westerly respectively in the western part of the WNP (Fig. 4e).

There are enhanced TC geneses in the western WNP during positive AMM phases (Fig. 3b). Such TC geneses are associated with weakened ZVWS in this region. The weakened ZVWS is caused by the displaced Walker circulation (Fig. 4e). The altered Walker circulation tends to weaken the prevalent upper easterly and it also weakens the lower westerly to some degree, resulting in weakened ZVWS in the western WNP (Fig. 4d, e). A number of studies have found that Atlantic SST anomalies could

Fig. 2 **a** The observed time series of WNP TC frequency (unit: times) and AMM index, and **b** the fitted lines of AMM and WNP TC frequency during 1970–2013 and neutral ENSO years in this period



act to modulate the Pacific Walker circulation and trades in the tropical Pacific by displacing the Walker circulation (Kucharski et al. 2011; Ham et al. 2013; McGregor et al. 2014), providing a plausible mechanism for the relationships observed in this section.

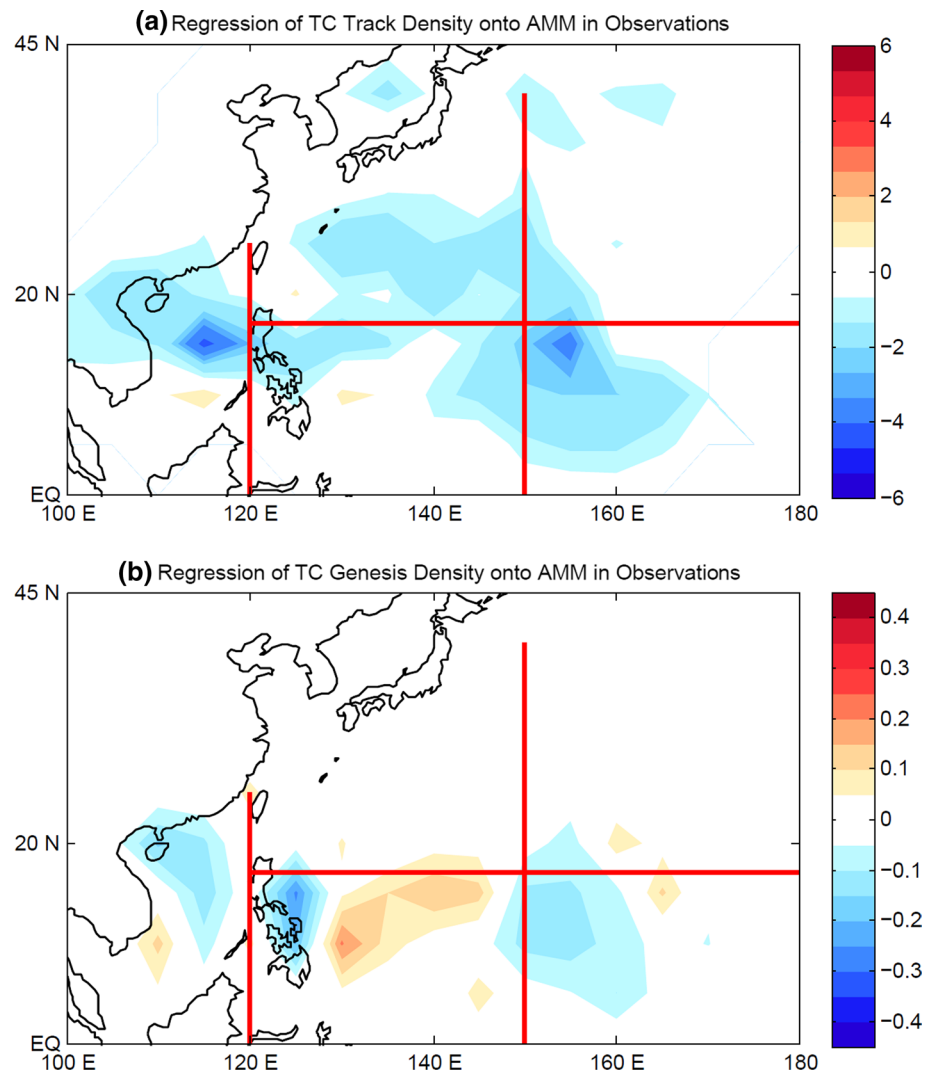
3.2 Control experiments

To investigate the mechanisms connecting the AMM and WNP TCs, we first assess whether the TC-AMM association holds in the long-term control experiment in a coupled climate model (FLOR-FA 1860). The fundamental structures of the observed AMM mode (i.e., a dipole mode of SST coupled with surface winds) are captured in the long-term control experiment of FLOR-FA (Fig. 5) as they were

in a related model (GFDL CM2.5) (Doi et al. 2013). Previous studies have found that the positive and negative SST anomalies related to AMM are not strongly connected to one another (e.g., Chiang and Vimont 2004). This is also consistent with the interpretation of meridional mode as an extratropics-to-tropics linkage (Chiang and Vimont 2004; Smirnov and Vimont 2012; Zhang et al. 2014).

Figure 6 depicts the histogram of the correlation coefficients between WNP TC frequency and the AMM index in every 45-year chunk of the 1000-year control simulation. The mean of the correlation coefficients is around -0.21 which is statistically different from 0 at 0.01 level of significance based on the Student's *t* test. (Figure 6), although the simulated WNPTC-AMM association is weaker than the observed one (the red vertical line in Fig. 6).

Fig. 3 Regression of WNP TC track **a** and genesis **b** density (unit: times) onto the AMM index in observations. The TC track/genesis density is defined as those binned into every $5^\circ \times 5^\circ$ grid box without smoothing. The *red lines* divides the WNP into five sub-domains: SCS, NW, SW, NE, and SE in the long-term control experiment with FLOR



For further analysis, we classify the 1000 years into the positive and negative AMM years with the magnitude of AMM index averaged over JJASON larger than one standard deviation. There are significantly fewer WNP TCs during the positive AMM years compared to the negative AMM years (Fig. 7). The anomalies of WNP TC frequency are defined as the deviation from the average WNP TC frequency over the 1000 years. The TC frequency difference in the southeastern portion of the WNP is mainly responsible for the difference in total WNP TC frequency between two AMM phases (Fig. 7), consistent with the observed spatial pattern of TC genesis (Fig. 3). The regression of TC track density onto the AMM index is characterized by negative anomalies in the WNP; on the other hand, the regression of TC genesis density in the long-term control experiment has characteristic negative anomalies only in the southeastern portion of the WNP with weak positive anomalies in its southwestern portion (Fig. 8). The positive anomalies in TC genesis in the southwestern part of WNP

in the control experiment is weaker than those in the observations (Figs. 3 and 8).

To disentangle the physical mechanisms underlying how AMM modulates WNP TC activity in the control experiment, we also regress the genesis potential index (GPI), 600-hPa relative humidity, 850-hPa relative vorticity, ZVWS and vertical atmospheric velocity onto AMM during strong AMM years as what is shown for observations. The regression of the GPI pattern onto AMM is consistent with the pattern of TC genesis (Figs. 8b, 9a). Among the key atmospheric variables relevant to GPI, ZVWS stands out to be linked with GPI because of the similarity in the regression of ZVWS and GPI onto AMM (Fig. 9). Previous studies have highlighted the key role of ZVWS in modulating TC genesis in the WNP (Wang and Chan 2002; Chan and Liu 2004), supporting our results both in the observations and long-term control experiment of FLOR-FA.

We find that ZVWS is changed mostly by the displacement of the Walker circulation in the WNP in the observations.

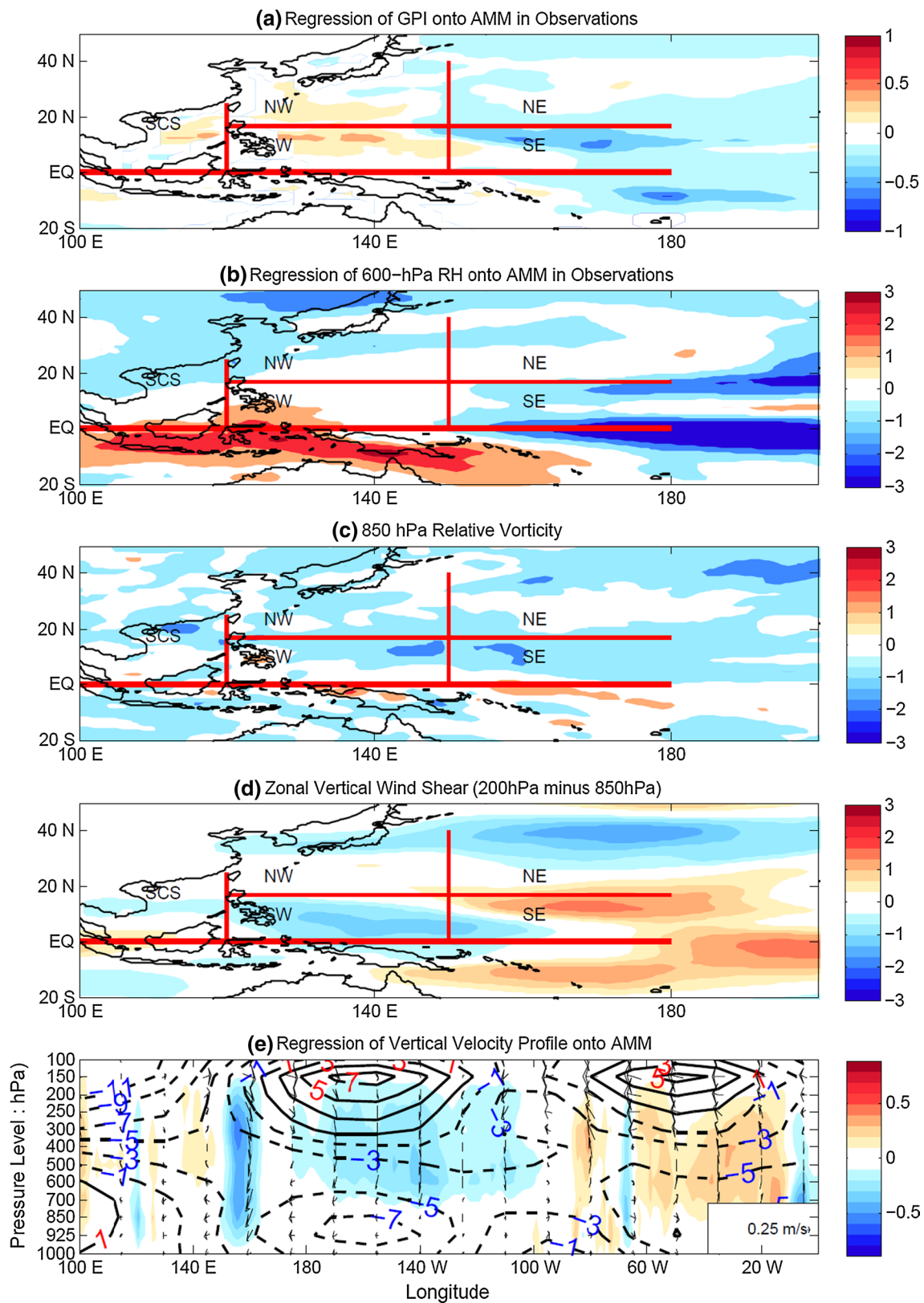


Fig. 4 Regression of GPI, 600 hPa relative humidity (unit: percent), 850 relative vorticity (unit: 10^{-6}s^{-1}), zonal vertical wind shear (unit: m/s), and vertical profile (0–20°N) of zonal wind (m s^{-1}) and vertical velocity ($-100*\omega$, Pa s^{-1}) onto the detrended AMM index. The

shading represents minus omega ($-\omega$). The red lines divide the WNP into five subdomains: SCS, NW, SW, NE, and SE. Contours in bottom panel represent the climatology of zonal wind (unit: m/s)

Fig. 5 Regression of SST (unit: $^{\circ}\text{C}$) and 10 m wind fields (ms^{-1}) onto the AMM index in the long-term control experiment with FLOR-FA

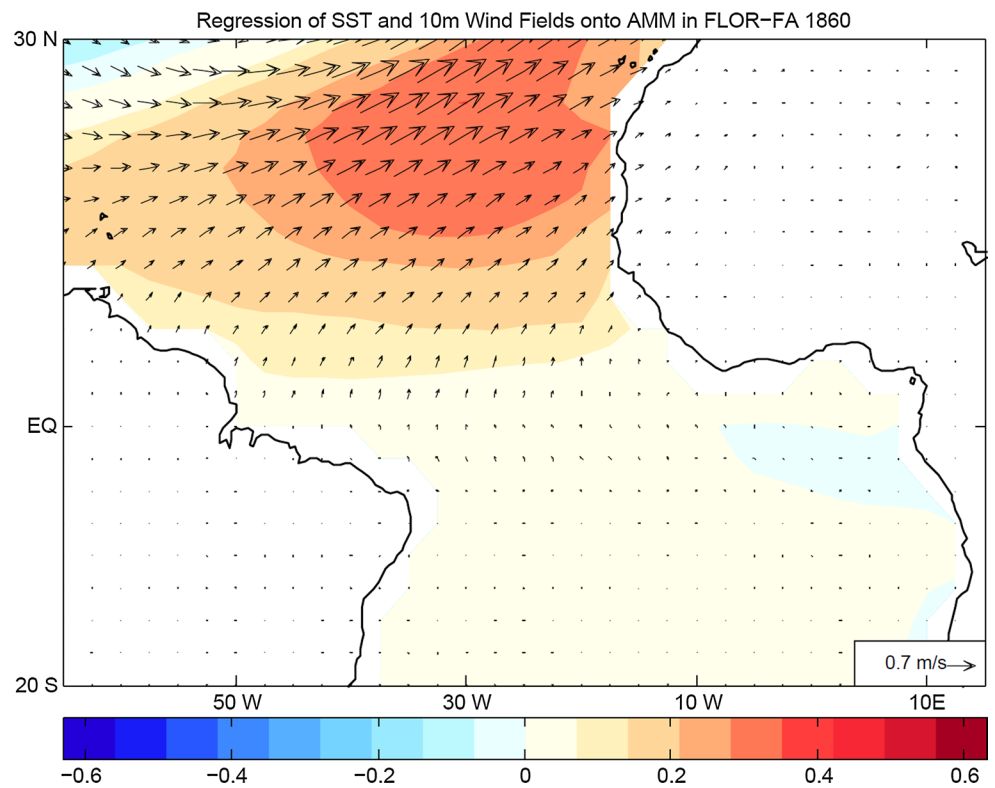


Fig. 6 The histogram of correlation coefficient between WNP TC frequency (unit: times) and the AMM index in every 45-year sub-periods in the 1860 (pre-industrial) control experiment with FLOR-FA. The red bar denotes the observed TC-AMM association

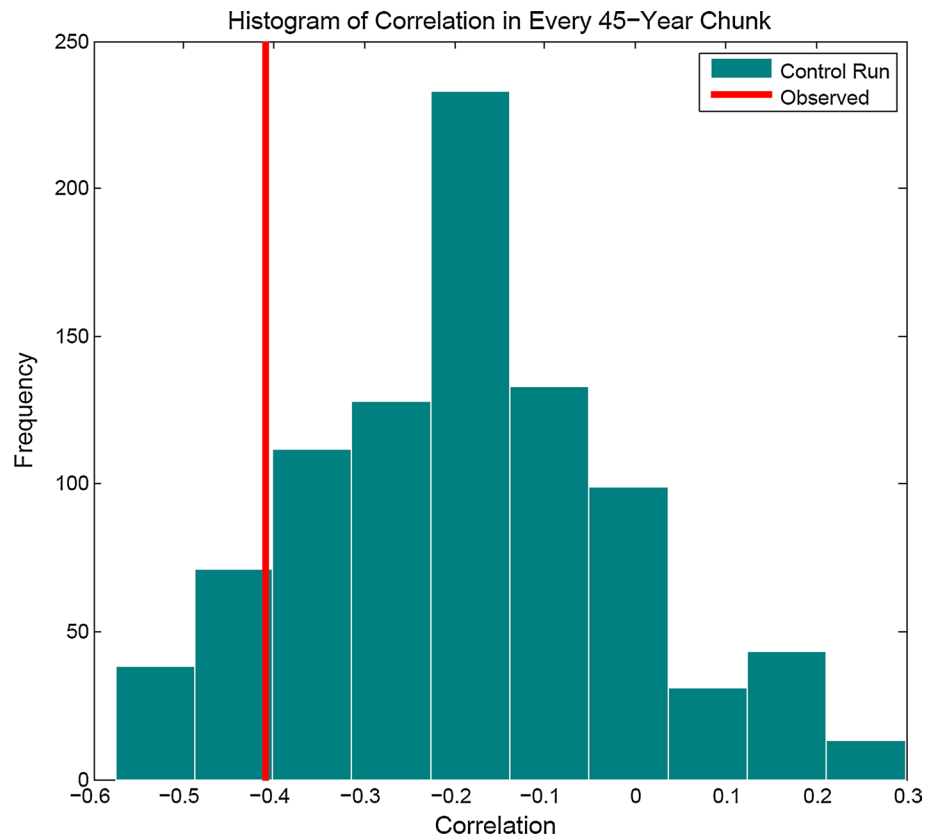


Fig. 7 The anomalous TC frequency in the WNP and its sub-domains (i.e., SCS, NW, SW, SE and NE as in Figs. 3, 4) during positive (blue) and negative (red) AMM years. The error bars represent the 0.95 confidence intervals. The symbol “asterisks” following the names of the sub-regions (e.g., WNP and SCS) below x-axis indicates that the differences between negative and positive AMM years are significant at 0.05 level of significance

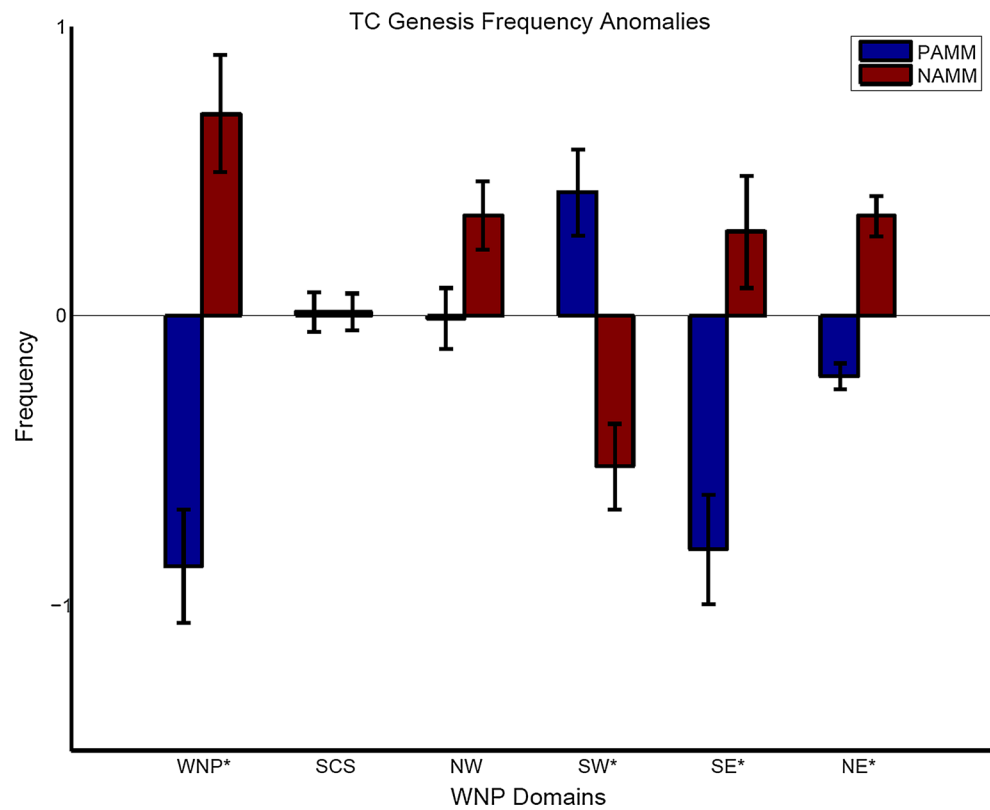


Figure 9e shows that an anomalous Walker cell resides from the eastern part of the WNP to the eastern Pacific (140°E to 100°W). To the east of this Walker cell, there is another anomalous Walker cell with descending branch located around 100°W , which is associated with the warming during positive AMM phase (Fig. 9e). We speculate that the AMM induces a displacement of the Walker circulation, which is responsible for changes in ZVWS in the WNP including strengthened ZVWS in the eastern WNP and weakened ZVWS in the western WNP (Fig. 9e). The climatology of zonal wind in control experiment is similar to that in observations (Figs. 4e, 9e). The altered Walker circulation is responsible for the intensified ZVWS in the eastern WNP by strengthening the prevalent (climatological) upper level westerly and lower level easterly and for the diminished ZVWS in the western WNP by weakening the prevalent (climatological) upper level easterly and lower level westerly (Fig. 9e). The anomalous ZVWS subsequently modulates WNP TC genesis. Such mechanisms are consistent with those based on observations. A suite of experiments using the state-of-the-art GFDL FLOR-FA coupled climate model are performed to verify the mechanisms underlying how AMM regulates WNP TC genesis.

3.3 Sensitivity experiments

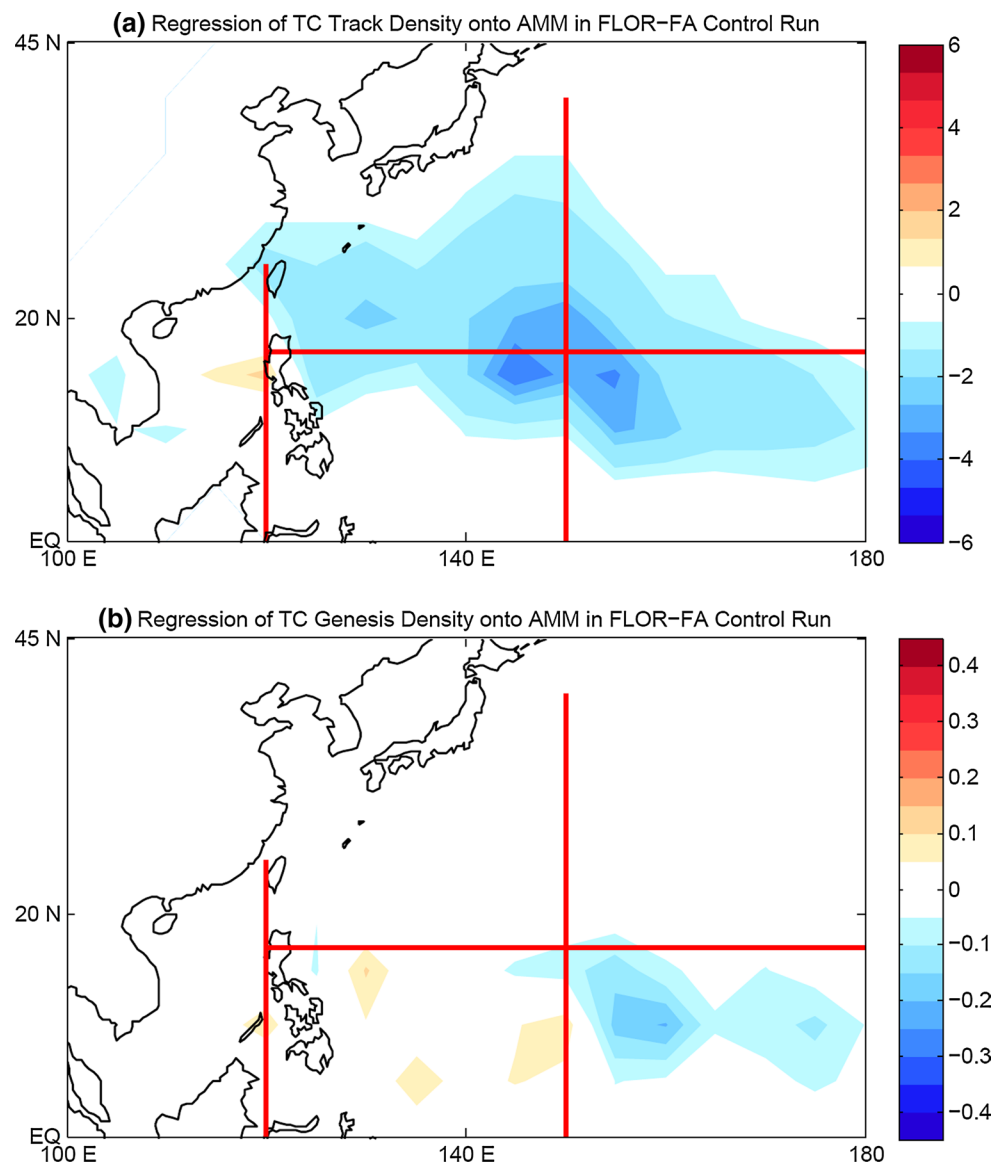
To verify the mechanisms underlying how the AMM influences TC activity in the WNP, we have performed a suite of

experiments including the control experiment and the perturbation experiment using FLOR-FA (Vecchi et al. 2014; Jia et al. 2015; Yang et al. 2015). The control and perturbation experiments are denoted as CLIMO and PAMM, respectively. The details of both experiments are provided in Sect. 2.

The PAMM experiment produces significantly fewer (3.7 times) WNP TCs than the CLIMO experiment (Table 1). It appears that the suppressed WNP TC genesis in the PAMM experiment is due to suppressed TC activity in the southeastern part of the WNP (Table 1). In addition, TC genesis in the northeastern part is also suppressed in the PAMM phases, even though the PAMM experiment produces more TC geneses in the southwestern part of the WNP (Table 1). Such forced TC responses are further supported by the differences in the spatial pattern of TC track and genesis density between PAMM and CLIMO experiments (Fig. 10).

The forced anomalous TC density responses to PAMM strongly resemble that in the long-term control experiment (Fig. 10a), though there are some weak positive TC density anomalies from the Philippines to Vietnam in the PAMM experiment. The subtraction of TC genesis density in the PAMM from CLIMO experiment produces anomalous negative anomalies in the eastern WNP and positive anomalies in a large portion of the western WNP, consistent with the observed TC genesis density anomalies in

Fig. 8 Regression of TC track and genesis density (unit: times) onto the AMM index during strong AMM years when the magnitude of the AMM index is larger than one standard deviation. The *red lines* divides the WNP into five sub-domains: SCS, NW, SW, NE, and SE in the long-term control experiment with FLOR



the observations (Figs. 3b, 10b). The negative TC genesis density anomalies in PAMM are located slightly eastward compared to the observations and this may be caused by the biases in simulated TC track density with FLOR or CM2.5 (Kim et al. 2014; Vecchi et al. 2014). The differences in the spatial pattern of TC genesis between PAMM and CLIMO experiments (Fig. 10) are consistent with what shown in Table 1. The PAMM experiment has less TC geneses in the southeastern portion and more TC geneses in the southwestern portion of the WNP than the CLIMO experiment (Fig. 10b), consistent with the results based on observations and the long-term control run with FLOR-FA.

To assess the role of key large-scale environmental variables in WNP TC genesis, we have analyzed the differences in GPI, relative humidity, 850 hPa relative vorticity,

ZVWS and the Walker circulation between PAMM and CLIMO experiments (Fig. 11). The sensitivity experiments reproduce the relationship between key variables and GPI in observations and long-term control experiment (Figs. 4, 9, 11). Negative GPI anomalies are located in the southeastern WNP while positive GPI anomalies are located in the southwestern WNP (Fig. 11a). The ZVWS differences between PAMM and CLIMO are characterized by positive anomalies in the southeastern WNP and negative anomalies in the southwestern WNP (Fig. 11d), consistent with the spatial patterns of GPI (Fig. 11a). The anomalous Walker circulation in the PAMM experiment shows similarity with what shown in the observations: there is an anomalous ascending branch in the Atlantic and a descending branch in the central Pacific forced by warming during the positive

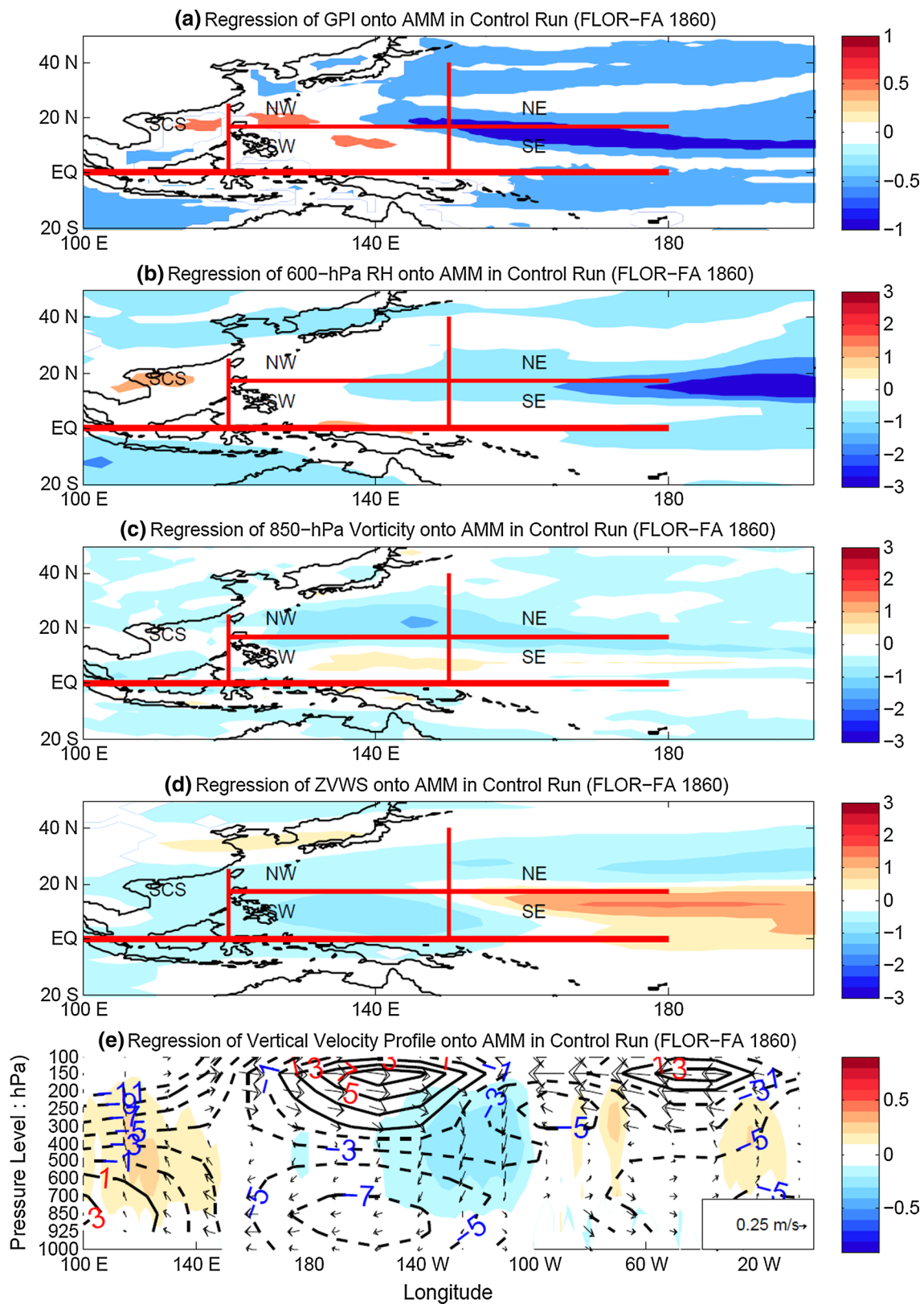


Fig. 9 Regression of GPI, 600 hPa relative humidity (unit: percent), 850 relative vorticity (unit: $10^{-6}s^{-1}$), zonal vertical wind shear (unit: m/s), and vertical profile (0–20°N) of zonal wind ($m s^{-1}$) and vertical velocity ($-100*\omega$, $Pa s^{-1}$) onto the AMM index in the WNP in the long-term

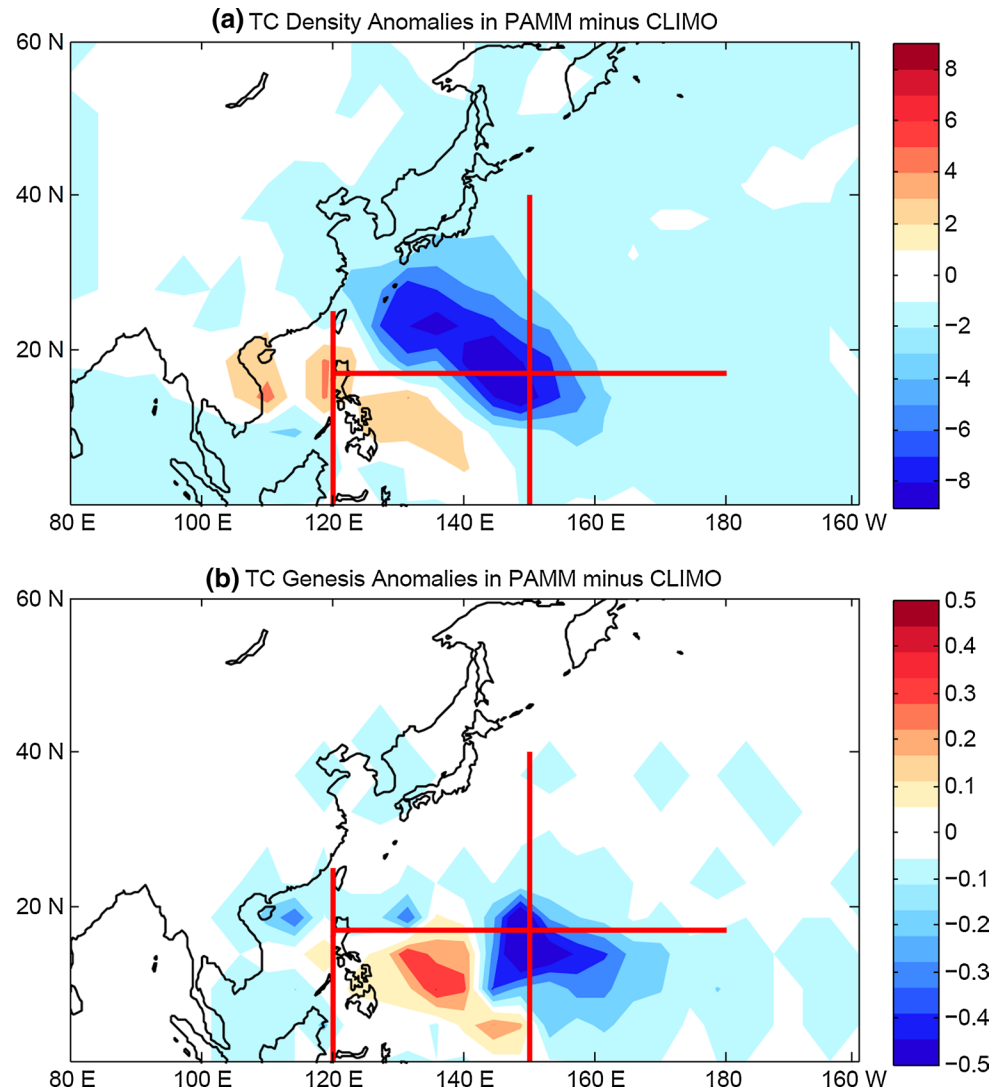
control experiment with FLOR. The shading represents minus omega ($-\omega$). The red lines divides the WNP into five sub-domains: SCS, NW, SW, NE, and SE in the long-term control experiment with FLOR. Contours in bottom panel represent the climatology of zonal wind (unit: m/s)

Table 1 TC frequency in the WNP and its sub-regions during peak season (JJASON) produced by the control experiment (CLIMO) and the perturbation experiment (PAMM)

TC Count	WNP	SCS	NW	SW	SE	NE
PAMM	19.9	2.4	3.2	11.4	2.4	0.5
CLIMO	23.6	2.8	4.1	9.9	5.5	1.3
Diff	-3.7*	-0.4	-0.9*	1.5*	-3.1*	-0.8*

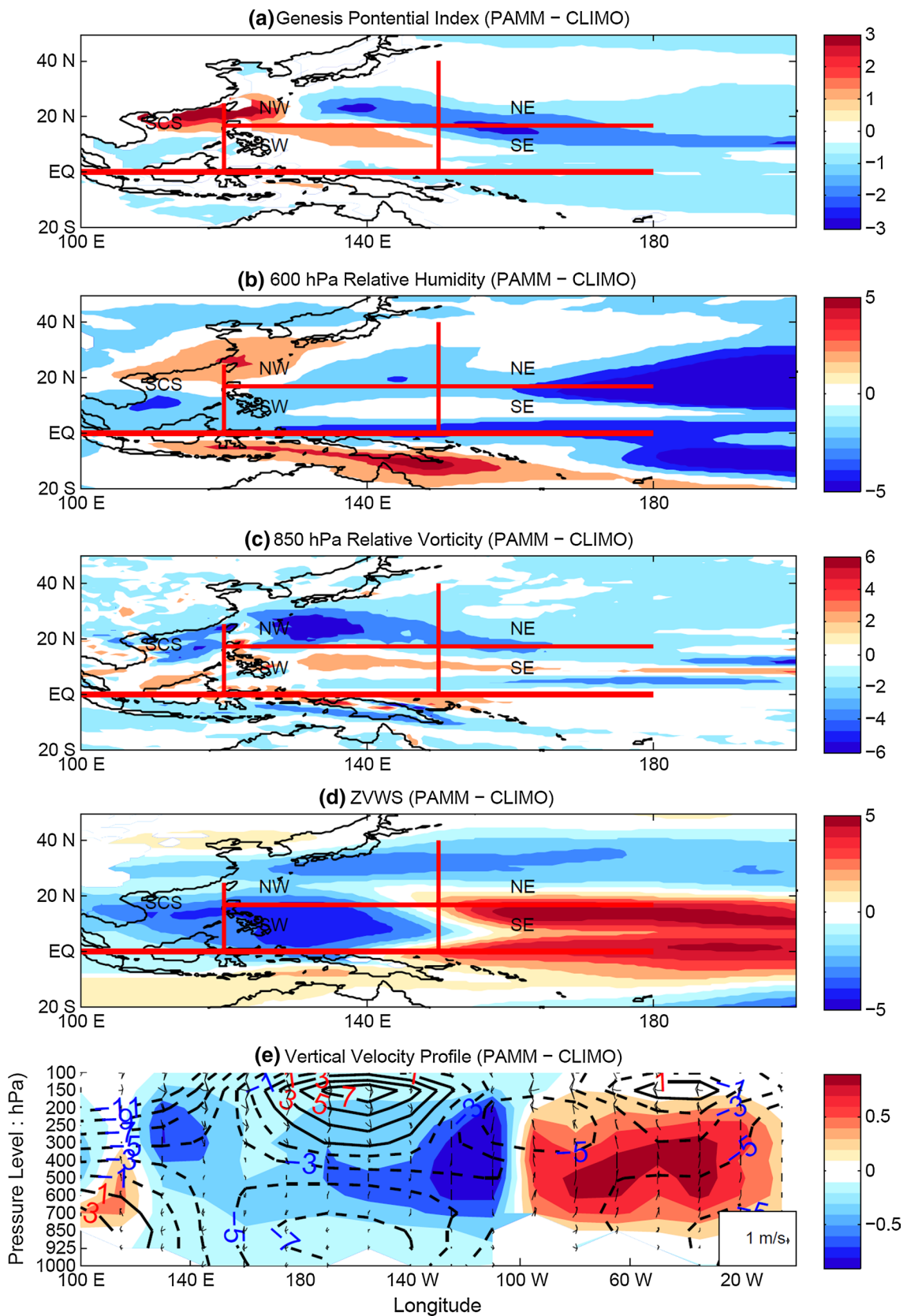
The boldface and “*” represent results that are significant at the 0.01 level

Fig. 10 The differences in WNP TC track and genesis density between PAMM and CLIMO experiments. The TC track/genesis density is obtained by binning TCs into every 5×5 grid box without smoothing. The *red lines* divides the WNP into five sub-domains: SCS, NW, SW, NE, and SE in the long-term control experiment with FLOR



AMM phases, which act to enhance the ascending branch in the eastern WNP (Fig. 11e). Such displacement of the Walker circulation leads to the anomalous Walker cell residing from the western to tropical central Pacific; this is responsible for the enhanced ZVWS in the eastern part of WNP and the diminished ZVWS in the western part of the WNP during the positive AMM phase (Fig. 11e). The anomalous Walker circulation in PAMM is located in a

Fig. 11 Differences in GPI, 600 hPa relative humidity (unit: percent), 850 relative vorticity (unit: 10^{-6}s^{-1}), zonal vertical wind shear (unit: m/s), and vertical profile (0–20°N) of zonal wind (m s^{-1}) and vertical velocity ($-100^* \omega$, Pa s^{-1}) between the PAMM and CLIMO experiments with FLOR-FA. The contours in *bottom panel* (e) represent the climatology of zonal wind (unit: m/s) in the CLIMO experiment. The *shading* represents minus omega ($-\omega$). The *red lines* divides the WNP into five sub-domains: SCS, NW, SW, NE, and SE in the long-term control experiment with FLOR



slightly different location compared to the observations. For example, the descending branch of the Walker circulation in the western WNP resides slightly westward compared with observations (Figs. 4e, 10e).

The two experiments (CLIMO and PAMM) therefore strongly support the physical mechanisms underlying the observed AMM-TC association. During the positive AMM phases, the anomalous SST warming in the North Atlantic forces changes in the atmospheric Walker circulation, which intensifies ZVWS in the eastern part of the WNP and suppresses TC genesis there.

4 Discussion and conclusion

Several studies have highlighted the important role of the North Atlantic SST in modulating WNP TC activity (e.g., Huo et al. 2015; Yu et al. 2015). The forcing impacts of remote tropical SST on TC activity have been identified in the North Atlantic and WNP (Vecchi and Soden 2007; Lin and Chan 2015). This study further examines the possible year-to-year modulation of WNP TC activity by AMM. Our research findings are summarized as follows.

1. The positive (negative) AMM phase suppresses (enhances) WNP TC activity in the observations. The anomalous occurrence of WNP TCs results mainly from changes in TC genesis in the southeastern part of the WNP.
2. The observed responses of WNP TC activity to the AMM phase are connected to the anomalous ZVWS driven by AMM-induced changes to the Walker circulation. During the positive AMM phase, the warming in the North Atlantic induces strong descending flow in the tropical eastern and central Pacific, which intensifies the Walker cell in the eastern WNP. The intensified Walker cell is responsible for the suppressed TC genesis in the eastern part of the WNP by strengthening ZVWS.
3. The observed WNPTC-AMM linkage is supported by the long-term control and idealized perturbations experiment with FLOR-FA. A suite of sensitivity experiments strongly corroborate the observed WNPTC-AMM linkage and underlying physical mechanisms.

The WNPTC-AMM linkage will provide useful references for seasonal prediction of WNP TC frequency by combining with other factors such as PMM, Niño 4 and the South Oscillation Index (Chan et al. 2001; Fan and Wang 2009). This study has identified the important role of AMM in mediating WNP TC activity, confirming the impacts of the Atlantic SST on WNP TCs (Huo et al. 2015; Yu et al.

2015). AMM influences WNP TC activity via changing ZVWS in the WNP (especially in the southeastern and southwestern portions) by altering the Walker circulation. Such physical mechanisms are strongly supported by previous studies. The Atlantic warming can induce the circulation changes that strengthen the trade winds by altering the Walker circulation using perturbation experiments (England et al. 2014; McGregor et al. 2014; Li et al. 2015). By forcing the atmosphere with positive anomalies in the Atlantic similar to the PAMM with warming in the North Atlantic, McGregor et al. (2014) have found similar responses of changes in the Walker circulation and trade winds. Kucharski et al. (2011, 2016) found that the physical mechanism for the Atlantic warming influence on the tropical Pacific is a change in the Walker circulation that results in easterly surface wind anomalies in the central-west Pacific. Kang et al. (2014) also found that AMO is related to changes of the SST cooling in the eastern and central Pacific accompanied by the easterly wind stress anomalies in the equatorial central Pacific, which were reproduced reasonably well by coupled general circulation model simulations performed with the Atlantic Ocean SST nudged with the observed SST representing the positive phase of the AMO. Therefore, this study has also proposed new physical mechanisms to interpret the linkage between AMM and WNP TC activity. Such underlying mechanisms are supported by observations, long-term control experiments and a suite of sensitivity experiments with the state-of-the-art FLOR-FA coupled climate model.

TC Frequency in the WNP has sharply decreased since the late 1990s (Tu et al. 2009; Liu and Chan 2012; Choi et al. 2015; He et al. 2015; Lin and Chan 2015). Such changes have been attributed to suppressed TC genesis in the southeastern part of the WNP (Liu and Chan 2012; He et al. 2015; Lin and Chan 2015; Wu et al. 2015). The Atlantic SST has been warming since 1950s and the multi-decadal change of the Atlantic SST (e.g., AMO) plays an important role in the rising SST. Based on our research findings, the suppressed TC activity in the WNP may be caused by the rising SST in the North Atlantic since the mid-1990s. This will be examined in our future work. PMM also exerts strong impacts on WNP TC activity (Zhang et al. 2016a). PMM enhances TC genesis in the WNP, especially in the southeastern WNP by inducing the Matsuno-Gill responses to the heating relevant to the northwestern part of the positive PMM pattern. Our ongoing research is examining how concurrent AMM and PMM influence WNP TC activity.

Despite the advancements made in understanding WNP TC activity, there are several caveats to be addressed. First, this study is limited by the uncertainties and biases in the simulations of FLOR-FA. Second, due to the inherent complexity existing in WNP TC activity, AMM is just

one factor/mode that modulates WNP TCs. The concurrent influences of AMM, PMM, ENSO and even East Indian Ocean SST on WNP TCs should be considered to obtain a more comprehensive understanding.

Acknowledgments The authors are grateful to Jim Kossin and an anonymous reviewer for their insightful comments that improve this paper. The authors thank Lakshmi Krishnamurthy and Honghai Zhang for their comments that improve an earlier version of this manuscript. This material is based in part upon work supported by the National Science Foundation under Grants AGS-1262091 and AGS-1262099.

Appendix

TCs in FLOR are tracked from 6-hourly model output by using the tracker developed at GFDL and this tracker has been implemented in Murakami et al. (2015) and Zhang et al. (2016a, b). The temperature anomaly averaged vertically over 300 and 500 hPa (t_a), 10 m wind speed, 850 hPa relative vorticity and sea level pressure (SLP) are key factors of this tracker. The tracking procedures are as follows.

1. Find local minima of the smoothed SLP field. The location of the cyclone center is properly adjusted by fitting a biquadratic surface to the SLP and locating the center at the minima.
2. Closed contours are in an interval of 2 hPa (dp) around every single low center. The N^{th} contour is marked as the contiguous region surrounding a low central pressure P with pressures lower than $dp \times N + P$, as detected by a “flood fill” algorithm. Note that the contours are not required to be circular and a maximum radius of 3,000 km is searched from each candidate SLP low center.
3. If the above closed contours are found, the low is counted as a TC center. In this way, the tracker attempts to find all closed contours within a certain distance of the low center and without entering contours belonging to another low. The maximum 10-m wind inside the set of closed contours is taken as the maximum wind speed at that time for the storm.
4. Warm cores are detected via similar processes: closed 1 K contours are found surrounding the maximum t_a within a TC’s identified contours, no more than 1 degree from the low center. This contour must have a radius smaller than 3 degrees in distance. If such a core is not found, it is not considered as a warm-core low center and the center is rejected.
5. TC centers are combined into a TC track by taking a low center at time $T-dt$, extrapolating its motion forward dt , and then seeking for storms within 750 km. A deeper low center has higher priority of tracking.
6. The following criteria are required to finalize the TC identifications.
 - (a) At least 72 h of total detection lifetime (not necessarily consecutive).
 - (b) At least 48 cumulative (not necessarily consecutive) hours with a warm core.
 - (c) At least 36 consecutive hours of a warm core with winds greater than 17.5 ms^{-1} .
 - (d) TC genesis should be confined equatorward of 40°N .

TC track/genesis density in the WNP is binned into $5^\circ \times 5^\circ$ grid boxes at a 6-h interval without smoothing.

References

- Camargo SJ, Sobel AH (2005) Western North Pacific tropical cyclone intensity and ENSO. *J Clim* 18:2996–3006
- Camargo SJ, Emanuel KA, Sobel AH (2007a) Use of a genesis potential index to diagnose ENSO effects on tropical cyclone genesis. *J Clim* 20:4819–4834
- Camargo SJ, Sobel AH, Barnston AG, Emanuel KA (2007b) Tropical cyclone genesis potential index in climate models. *Tellus A* 59:428–443
- Carton JA, Cao X, Giese BS, Da Silva AM (1996) Decadal and interannual SST variability in the tropical Atlantic Ocean. *J Phys Oceanogr* 26:1165–1175
- Chan JCL (1985) Tropical cyclone activity in the Northwest Pacific in relation to the El Niño Southern Oscillation phenomenon. *Mon Weather Rev* 113:599–606
- Chan JCL (2000) Tropical cyclone activity over the western North Pacific associated with El Niño and La Niña events. *J Clim* 13:2960–2972
- Chan JCL, Liu KS (2004) Global warming and western North Pacific typhoon activity from an observational perspective. *J Clim* 17:4590–4602
- Chan JCL, Shi J, Liu KS (2001) Improvements in the seasonal forecasting of tropical cyclone activity over the Western North Pacific. *Weather Forecast* 16:491–498
- Chang P, Ji L, Li H (1997) A decadal climate variation in the tropical Atlantic Ocean from thermodynamic air–sea interactions. *Nature* 385:516–518
- Chiang JCH, Vimont DJ (2004) Analogous Pacific and Atlantic Meridional Modes of tropical atmosphere–ocean variability*. *J Clim* 17:4143–4158
- Chiang JCH, Kushnir Y, Giannini A (2002) Deconstructing Atlantic intertropical convergence zone variability: influence of the local cross-equatorial sea surface temperature gradient and remote forcing from the eastern equatorial Pacific. *J Geophys Res Atmos* 107:ACL 3-1–ACL 3-19
- Choi Y, Ha K-J, Ho C-H, and Chung C (2015) Interdecadal change in typhoon genesis condition over the western North Pacific. *Clim Dyn* 45:3243–3255
- Delworth TL, Broccoli AJ, Rosati A, Stouffer RJ, Balaji V, Beesley JA, Cooke WF, Dixon KW, Dunne J, Dunne KA, Durachta JW, Findell KL, Ginoux P, Gnanadesikan A, Gordon CT, Griffies

- SM, Gudgel R, Harrison MJ, Held IM, Hemler RS, Horowitz LW, Klein SA, Knutson TR, Kushner PJ, Langenhorst AR, Lee H-C, Lin S-J, Lu J, Malyshev SL, Milly PCD, Ramaswamy V, Russell J, Schwarzkopf MD, Shevliakova E, Sirutis JJ, Spelman MJ, Stern WF, Winton M, Wittenberg AT, Wyman B, Zeng F, Zhang R (2006) GFDL's CM2 global coupled climate models. Part I: formulation and simulation characteristics. *J Clim* 19:643–674
- Delworth TL, Rosati A, Anderson W, Adcroft AJ, Balaji V, Benson R, Dixon K, Griffies SM, Lee H-C, Pacanowski RC, Vecchi GA, Wittenberg AT, Zeng F, Zhang R (2012) Simulated climate and climate change in the GFDL CM2.5 high-resolution coupled climate model. *J Clim* 25:2755–2781
- Deser C, Wallace JM (1987) El Niño events and their relation to the Southern Oscillation: 1925–1986. *J Geophys Res Oceans* 92:14189–14196
- Doi T, Vecchi GA, Rosati AJ, Delworth TL (2013) Response to CO₂ doubling of the Atlantic hurricane main development region in a high-resolution climate model. *J Clim* 26:4322–4334
- Du Y, Yang L, Xie S-P (2010) Tropical Indian Ocean influence on northwest Pacific tropical cyclones in summer following strong El Niño*. *J Clim* 24:315–322
- Emanuel KA and Nolan D (2004) Tropical cyclone activity and the global climate system. Preprints, 26th conference on hurricanes and tropical meteorology. American Meteorological Society A, Miami, FL
- England MH, McGregor S, Spence P, Meehl GA, Timmermann A, Cai W, Gupta AS, McPhaden MJ, Purich A, Santoso A (2014) Recent intensification of wind-driven circulation in the Pacific and the ongoing warming hiatus. *Nat Clim Change* 4:222–227
- Fan K, Wang H (2009) A new approach to forecasting typhoon frequency over the western North Pacific. *Weather Forecast* 24:974–986
- Girishkumar MS, Thanga Prakash VP, Ravichandran M (2014) Influence of Pacific decadal oscillation on the relationship between ENSO and tropical cyclone activity in the Bay of Bengal during October–December. *Clim Dyn* 44:3469–3479
- Gray WM (1979) Hurricanes: their formation, structure and likely role in the tropical circulation. *Meteorol Trop Oceans* 77:155–218
- Grossmann I, Klotzbach PJ (2009) A review of North Atlantic modes of natural variability and their driving mechanisms. *J Geophys Res* 114:D24107. doi:10.1029/2009JD012728
- Ham Y-G, Kug J-S, Park J-Y, Jin F-F (2013) Sea surface temperature in the north tropical Atlantic as a trigger for El Niño/Southern Oscillation events. *Nat Geosci* 6:112–116
- He H, Yang J, Gong D, Mao R, Wang Y, Gao M (2015) Decadal changes in tropical cyclone activity over the western North Pacific in the late 1990s. *Clim Dyn* 45:3317–3329
- Huo L, Guo P, Hameed SN, Jin D (2015) The role of tropical Atlantic SST anomalies in modulating western North Pacific tropical cyclone genesis. *Geophys Res Lett* 42:2378–2484
- Jia L, Yang X, Vecchi GA, Gudgel RG, Delworth TL, Rosati A, Stern WF, Wittenberg AT, Krishnamurthy L, Zhang S, Msadek R, Kaplan S, Underwood S, Zeng F, Anderson WG, Balaji V, Dixon K (2015) Improved seasonal prediction of temperature and precipitation over land in a high-resolution GFDL climate model. *J Clim* 28:2044–2062
- Kalnay E, Kanamitsu M, Kistler R, Collins W, Deaven D, Gandin L, Iredell M, Saha S, White G, Woollen J (1996) The NCEP/NCAR 40-year reanalysis project. *Bull Am Meteorol Soc* 77:437–471
- Kang I-S, No H-H, Kucharski F (2014) ENSO amplitude modulation associated with the mean SST changes in the tropical central Pacific induced by Atlantic Multidecadal Oscillation. *J Clim* 27:7911–7920
- Kennedy JJ, Rayner NA, Smith RO, Parker DE, Saunby M (2011) Reassessing biases and other uncertainties in sea surface temperature observations measured in situ since 1850: 2 Biases and homogenization. *J Geophys Res Atmos* 116:D14104
- Kim H-S, Vecchi GA, Knutson TR, Anderson WG, Delworth TL, Rosati A, Zeng F, Zhao M (2014) Tropical cyclone simulation and response to CO₂ doubling in the GFDL CM2.5 high-resolution coupled climate model. *J Clim* 27:8034–8054
- Klotzbach PJ (2007) Recent developments in statistical prediction of seasonal Atlantic basin tropical cyclone activity. *Tellus B Dyn Meteorol Oceanogr* 59:511–518
- Knapp KR, Kruk MC, Levinson DH, Diamond HJ, Neumann CJ (2010) The international best track archive for climate stewardship (IBTrACS). *Bull Am Meteorol Soc* 91:363–376
- Kobayashi S, Ota Y, Harada Y, Ebata A, Moriya M, Onoda H, Onogi K, Kamahori H, Kobayashi C, Endo H, Miyaoka K, Takahashi K (2015) The JRA-55 reanalysis: general specifications and basic characteristics. *J Meteorol Soc Jpn Ser II* 93:5–48
- Kossin JP, Vimont DJ (2007) A more general framework for understanding Atlantic hurricane variability and trends. *Bull Am Meteorol Soc* 88:1767–1781
- Kucharski F, Kang IS, Farneti R, Feudale L (2011) Tropical Pacific response to 20th century Atlantic warming. *Geophys Res Lett* 38:L03702. doi:10.1029/2010GL046248
- Kucharski F et al (2016) Atlantic forcing of Pacific decadal variability. *Clim Dyn*. doi:10.1007/s00382-015-2705-z
- Lee HS, Yamashita T, Mishima T (2012) Multi-decadal variations of ENSO, the Pacific Decadal Oscillation and tropical cyclones in the western North Pacific. *Prog Oceanogr* 105:67–80
- Li X, Yang S, Wang H, Jia X, Kumar A (2013) A dynamical-statistical forecast model for the annual frequency of western Pacific tropical cyclones based on the NCEP Climate Forecast System version 2. *J Geophys Res Atmos* 118:12061–12074
- Li X, Xie S-P, Gille ST, Yoo C (2015) Atlantic-induced pan-tropical climate change over the past three decades. *Nat Clim Change* 6:275–279
- Lin II, Chan JCL (2015) Recent decrease in typhoon destructive potential and global warming implications. *Nat Commun* 6:7182. doi:10.1038/ncomms8182
- Liu KS, Chan JCL (2012) Inactive period of western North Pacific tropical cyclone activity in 1998–2011. *J Clim* 26:2614–2630
- McGregor S, Timmermann A, Stuecker MF, England MH, Merrifield M, Jin F-F, Chikamoto Y (2014) Recent Walker circulation strengthening and Pacific cooling amplified by Atlantic warming. *Nat Clim Change* 4:888–892
- Mitchell CL (1932) West Indian hurricanes and other tropical cyclones of the North Atlantic Ocean. *Mon Weather Rev* 60:253
- Murakami H, Vecchi GA, Underwood S, Delworth T, Wittenberg AT, Anderson W, Chen J-H, Gudgel R, Harris L, Lin S-J, Zeng F (2015) Simulation and prediction of Category 4 and 5 hurricanes in the high-resolution GFDL HiFLOR coupled climate model. *J Clim* 28:9058–9079
- Nobre P, Shukla J (1996) Variations of sea surface temperature, wind stress, and rainfall over the tropical Atlantic and south America. *J Clim* 9:2464–2479
- Pielke R Jr, Gratz J, Landsea C, Collins D, Saunders M, Musulin R (2008) Normalized hurricane damage in the United States: 1900–2005. *Nat Hazards Rev* 9:29
- Rappaport EN (2000) Loss of life in the United States associated with recent Atlantic tropical cyclones. *Bull Am Meteorol Soc* 81:2065–2073
- Servain J (1991) Simple climatic indices for the tropical Atlantic Ocean and some applications. *J Geophys Res Oceans* 96:15137–15146
- Smirnov D, Vimont DJ (2011) Variability of the Atlantic Meridional Mode during the Atlantic hurricane season. *J Clim* 24:1409–1424
- Smirnov D, Vimont DJ (2012) Extratropical forcing of tropical Atlantic variability during the boreal summer and fall. *J Clim* 25:2056–2076

- Tu JY, Chou C, Chu PS (2009) The abrupt shift of typhoon activity in the vicinity of Taiwan and its association with western North Pacific-East Asian climate change. *J Clim* 22:3617–3628
- Vecchi GA, Soden BJ (2007) Effect of remote sea surface temperature change on tropical cyclone potential intensity. *Nature* 450:1066–1070
- Vecchi GA, Delworth T, Gudgel R, Kapnick S, Rosati A, Wittenberg AT, Zeng F, Anderson W, Balaji V, Dixon K, Jia L, Kim HS, Krishnamurthy L, Msadek R, Stern WF, Underwood SD, Villarini G, Yang X, Zhang S (2014) On the seasonal forecasting of regional tropical cyclone activity. *J Clim* 27:7994–8016
- Vimont DJ, Kossin JP (2007) The Atlantic Meridional Mode and hurricane activity. *Geophys Res Lett* 34:L07709
- Vitart FD, Stockdale TN (2001) Seasonal forecasting of tropical storms using coupled GCM integrations. *Mon Weather Rev* 129:2521–2537
- Wang B, Chan JCL (2002) How strong ENSO events affect tropical storm activity over the Western North Pacific. *J Clim* 15:1643–1658
- Wu GX, Lau NC (1992) A GCM simulation of the relationship between tropical–storm formation and ENSO. *Mon Weather Rev* 120:958–977
- Wu L, Wang C, Wang B (2015) Westward shift of western North Pacific tropical cyclogenesis. *Geophys Res Lett* 42:1537–1542
- Xie S-P, Philander SGH (1994) A coupled ocean-atmosphere model of relevance to the ITCZ in the eastern Pacific. *Tellus A* 46:340–350
- Yang X, Vecchi GA, Gudgel RG, Delworth TL, Zhang S, Rosati A, Jia L, Stern WF, Wittenberg AT, Kapnick S, Msadek R, Underwood SD, Zeng F, Anderson W, Balaji V (2015) Seasonal predictability of extratropical storm tracks in GFDL's high-resolution climate prediction model. *J Clim* 28:3592–3611
- Yu J-Y, Kao P-K, Paek H, Hsu H-H, Hung C-W, Lu M-M, An S-I (2014) Linking emergence of the central Pacific El Niño to the Atlantic multidecadal oscillation. *J Clim* 28:651–662
- Yu J, Li T, Tan Z, Zhu Z (2015) Effects of tropical North Atlantic SST on tropical cyclone genesis in the western North Pacific. *Clim Dyn* 46:865–877
- Zhan R, Wang Y, Lei X (2010) Contributions of ENSO and East Indian Ocean SSTA to the interannual variability of northwest Pacific tropical cyclone frequency*. *J Clim* 24:509–521
- Zhan R, Wang Y, Tao L (2014) Intensified impact of East Indian Ocean SST anomaly on tropical cyclone genesis frequency over the western North Pacific. *J Clim* 27:8724–8739
- Zhang R, Delworth TL (2007) Impact of the Atlantic multidecadal oscillation on North Pacific climate variability. *Geophys Res Lett* 34:L23708
- Zhang L, Zhao C (2015) Processes and mechanisms for the model SST biases in the North Atlantic and North Pacific: a link with the Atlantic meridional overturning circulation. *J Adv Model Earth Syst* 7:739–758
- Zhang Q, Liu Q, Wu L (2009) Tropical cyclone damages in China 1983–2006. *Bull Am Meteorol Soc* 90:489–495
- Zhang W, Graf HF, Leung Y, Herzog M (2012) Different El Niño types and tropical cyclone landfall in East Asia. *J Clim* 25:6510–6523
- Zhang W, Leung Y, Min J (2013) North Pacific Gyre Oscillation and the occurrence of western North Pacific tropical cyclones. *Geophys Res Lett* 40(19):5205–5211
- Zhang H, Deser C, Clement A, Tomas R (2014) Equatorial signatures of the Pacific meridional modes: dependence on the mean climate state. *Geophys Res Lett* 41:568–574. doi:[10.1002/2013GL058842](https://doi.org/10.1002/2013GL058842)
- Zhang W, Leung Y, Fraedrich K (2015) Different El Niño types and intense typhoons in the Western North Pacific. *Clim Dyn* 11–12:2965–2977
- Zhang W, Vecchi G, Murakami H, Villarini G, Jia L (2016a) The Pacific meridional mode and the occurrence of tropical cyclones in the Western North Pacific. *J Clim* 29:381–398
- Zhang W, Vecchi GA, Murakami H, Delworth T, Wittenberg AT, Anderson W, Rosati A, Underwood S, Harris L, Gudgel R, Lin S-J, Villarini G, Chen J-H (2016b) Improved simulation of tropical cyclone responses to ENSO in the Western North Pacific in the high-resolution GFDL HiFLOR coupled climate model. *J Clim* 29:1391–1415